

Near-field Optical Spectroscopy of Single GaAs Quantum Wires

A. Richter,¹ M. Süptitz,¹ Ch. Lienau,^{1,*} T. Elsaesser,¹ M. Ramsteiner,² R. Nötzel² and K. H. Ploog²

¹ Max-Born-Institut für Nichtlineare Optik und Kurzzeitspektroskopie, Rudower Chaussee 6, D-12489 Berlin, Germany

² Paul-Drude-Institut für Festkörperelektronik, Hausvogteiplatz 5-7, D-10117 Berlin, Germany

The nanoscopic room temperature optical properties of single quantum wires are characterized by a combination of near-field photoluminescence and photoluminescence excitation spectroscopy. Single GaAs quantum wires with a 50 nm lateral dimension are grown at the edge of 15 nm high mesa stripes on patterned GaAs(311) surfaces. Wire formation relies on the preferential migration of Ga atoms from a GaAs layer on the mesa top and bottom towards the sidewall. Spatially resolved photoluminescence spectra separate quantum wire and quantum well emission and image the diffusion of photoexcited carriers into the wires. Photoluminescence excitation spectra give insight into the absorption spectrum of the wires and the spectral position of different interband transitions in the one-dimensional carrier system. They allow the change in local thickness of the GaAs quantum well due to the migration process to be monitored directly with subwavelength spatial resolution. Both the trapping of carriers into the wire and the detrapping of carriers generated within the wire into the surrounding quantum well states are separately resolved. © 1997 by John Wiley & Sons, Ltd.

Surf. Interface Anal. 25, 583–592 (1997)

No. of Figures: 12 No. of Tables: 0 No. of Refs: 17

KEYWORDS: near-field microscopy; semiconductors; quantum wires; photoluminescence spectroscopy

INTRODUCTION

Semiconductor nanostructures play an important role in modern solid-state physics and are the basis of many optoelectronic devices. Until recently, research has mainly concentrated on quasi-two-dimensional structures like quantum wells (QW) and superlattices whose electronic and optical properties are understood in great detail. This includes the non-equilibrium dynamics of carriers and excitons occurring on ultrafast time scales. A further reduction of dimensionality to one- and zero-dimensional structures is of interest both from the viewpoint of fundamental physics and for device applications. Several concepts have been introduced to realize quasi-one-dimensional quantum wires (QWRs). Photolithography and subsequent deep mesa etching of QWs have been used to produce arrays of QWRs with a QWR width of about 400 nm.¹ Other systems make use of microstructured gate electrodes on top of a quasi-two-dimensional electron gas to generate a one-dimensional confinement. For instance, a laterally periodic modulated gate has been introduced in GaAs/AlGaAs heterojunctions, resulting in parallel 400–500 nm wide QWRs (For a review, see Ref. 2). Overgrowth techniques^{3–5} and epitaxial growth on prestructured substrates represent different approaches to realize one-dimensional semiconductors of high structural quality. In particular, QWRs on prestructured substrates show favourable optical properties, e.g. substantial lumines-

cence emission at room temperature. The growth of GaAs/AlGaAs QWs on GaAs substrates that are patterned with V-grooves results in a slight change of QW thickness at the bottom of the groove and thus a one-dimensional confinement of carriers over a width of ~50–100 nm.⁶ Very recently, QWRs of ~50 nm wide were formed along the sidewall of mesa stripes grown by molecular beam epitaxy (MBE) on patterned GaAs(311) substrates.^{7,8}

In most experiments, the electronic and optical properties of ensembles of up to hundreds of QWRs have been studied. In such cases, the optical spectra show a substantial inhomogeneous broadening originating from size fluctuations within the QWR array. In addition, there might be electromagnetic interactions between neighbouring wires. Both effects make a characterization of the one-dimensional behaviour quite difficult. The investigation of a single QWR by optical techniques of very high spatial resolution avoids this problem and should provide highly specific insight into the one-dimensional carrier system. Near-field scanning optical microscopy (NSOM) represents such a method allowing for a spatial resolution in the 100 nm range. Very recently, a first NSOM experiment on single QWRs has been reported and an enhancement of QWR-compared QW absorption was derived from the data.⁹

In this paper, we present the first NSOM study of single sidewall quantum wires grown on patterned GaAs(311) substrates. Both photoluminescence (PL) and photoluminescence excitation (PLE) spectra are measured at room temperature. The PL from the QWR and the surrounding QW are clearly separated in spatially resolved measurements, providing direct insight into diffusion and trapping of photoexcited carriers into

* Correspondence to: Ch. Lienau, Max-Born-Institut für Nichtlineare Optik und Kurzzeitspektroskopie, Rudower Chaussee 6, D-12489 Berlin, Germany.

the QWR. The PLE measurements give the energy position of the different QWR and QW transitions and compare very well with theoretical calculations of the one-dimensional band structure. Finally, our data demonstrate the occurrence of fast carrier exchange processes between QWR and QW driven by absorption and emission of longitudinal optical phonons.

The paper is organized as follows. After a description of our experimental techniques we recall results of microluminescence measurements from Ref. 7, allowing a first characterization of the different emission bands. The main part of the paper is devoted to NSOM studies of PL and PLE spectra and carrier exchange between one- and two-dimensional states, and conclusions are given in the final section.

EXPERIMENTAL

In NSOM, spatial resolution is achieved by transmitting light through a nanometre-sized aperture located at the end of a NSOM probe tip. The NSOM probe tips were made by pulling single-mode optical fibres to a sharp taper with a cone angle of 10° in a commercial CO_2 -laser-based fibre puller (Sutter) and then coating the taper with a 50–100 nm thick aluminium or gold layer. The diameter of the aperture at the very end of the taper was varied between < 50 and > 300 nm.

In this study, the near-field microscope was used in two different modes of operation. In the excitation mode [Fig. 1(a)], spatially resolved optical excitation of the sample was achieved by transmitting the excitation light through the aperture at the end of the NSOM probe tip. Photoluminescence emitted by the sample was then collected with a standard microscope objective in reflection geometry. The PL was dispersed in a 0.22 m double monochromator and detected with a single-photon-counting system based on a silicon avalanche photodiode detector (Si-APD). In the collection mode [Fig. 1(b)], the excitation laser was focused to a spot size of $\sim 50 \mu\text{m}$ and the PL was collected with the NSOM fibre probe, spectrally dispersed and detected with the Si-APD. In the experiments the PL is detected as a function of the tip position whilst the sample, which is mounted on a x - y - z -piezo, is scanned relative to the probe tip. During the scan, the tip-to-sample distance was kept constant at 5 ± 1 nm by adjusting the z -piezo voltage using a modified version of the optical shear force set-up proposed in Refs 10 and 11. Shear force images, i.e. images of the z -piezo voltage as a function of tip position, give direct information about the topography of the sample surface and were recorded simultaneously with the near-field PL images. The piezoscanner was software linearized and calibrated against a standard atomic force microscopy (AFM) grating with a calibration error of less than $\pm 5\%$. The scan range in these experiments was typically $10 \times 10 \mu\text{m}^2$, and 100×100 or 200×200 data points were recorded for each scan. A diode-pumped continuous wave $\text{Cr}^{3+}:\text{LiSAF}$ laser (Time Bandwidth Products) tunable between 810 and 860 nm and an HeNe laser were used as excitation sources. The power of the excitation light coupled into the fibre probe was ~ 3 mW and that of the light transmitted through the fibre tip

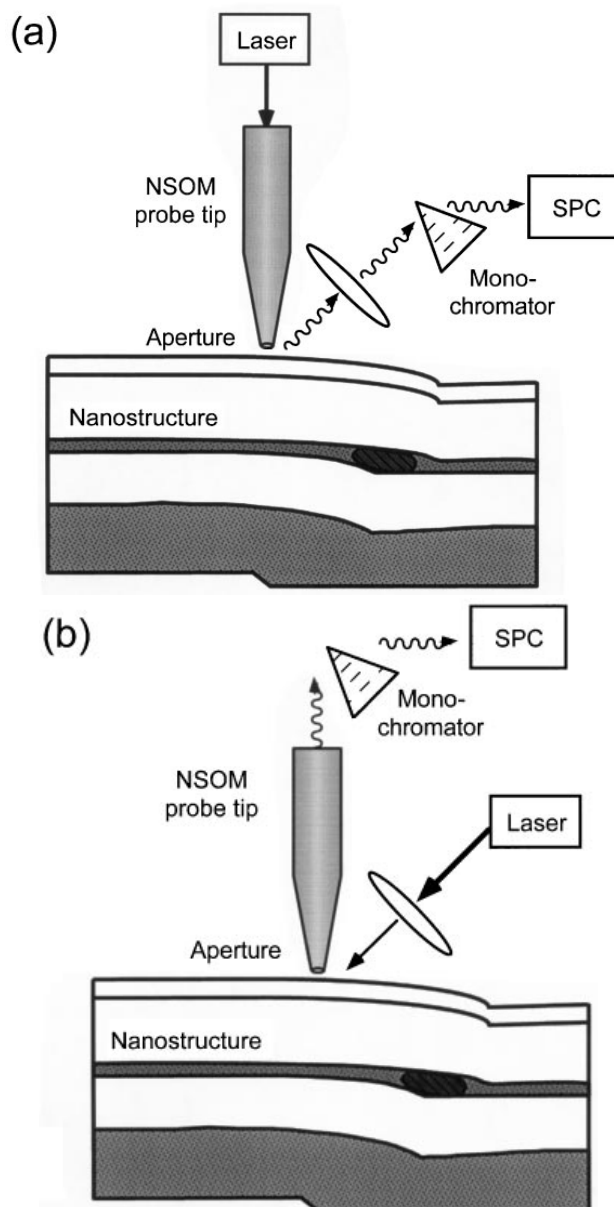


Figure 1. Schematic of the experimental set-up. Experiments have been performed in two different modes of the near-field microscope. (a) Excitation mode: spatially resolved excitation of the sample is achieved by transmitting light through a nanometre-sized aperture at the end of a near-field scanning optical microscopy (NSOM) probe tip. Photoluminescence is collected with a microscope, spectrally resolved in a double monochromator and detected with a single-photon-counting Si avalanche photodiode (SPC). The sample is mounted on an x - y - z stage and scanned relative to the tip. During the scan the tip to sample distance is kept constant at 5 nm by using an optical shear force setup. (b) Collection mode: after broad area excitation (laser focus diameter $\sim 50 \mu\text{m}$), spatially resolved photoluminescence is collected through the NSOM fibre probe, spectrally dispersed and detected.

onto the sample varied between 10 and 100 nW, depending on the tip diameter, when detected in the far field. At these excitation powers, heating of the fibre tip¹² did not influence the experiments.

The resolution obtained with our near-field microscope is demonstrated in Fig. 2. Shear force images recorded with uncoated fibre probes with a tip diameter of < 30 nm gave a lateral resolution of better than 12 nm, as demonstrated by imaging the oxidized surface of

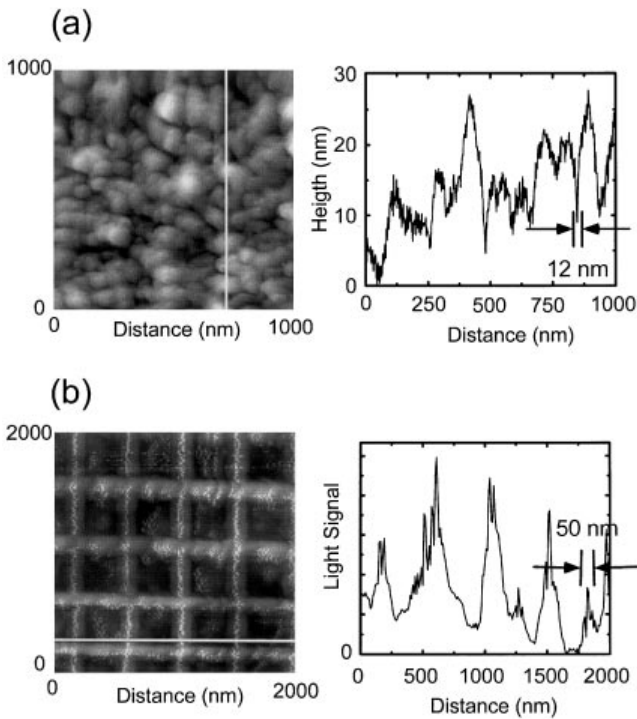


Figure 2. Resolution in near-field microscopy. (a) Topography of a GaAs laser diode recorded using shear force microscopy. The image was recorded with an uncoated tapered single-mode optical fibre with a tip diameter of <30 nm. The tip-to-sample distance was kept constant at 3 ± 1 nm. The lateral resolution is better than 12 nm, while the vertical resolution is better than 1 nm. (b) Reflection mode imaging of a standard atomic force microscopy (AFM) test grating. The distance between adjacent lines of the grating is kept constant at 3 ± 1 nm. The lateral resolution is better than 12 nm, while the vertical resolution is better than 1 nm. (b) Laser light transmitted through a metal-coated near-field scanning optical microscopy (NSOM) fibre probe with an aperture of <50 nm is reflected off the grating surface, collected with a microscope objective and detected with a photomultiplier. The reflected light intensity is shown as a function of tip position. A linescan along the line indicated in the two-dimensional picture shows structures that are narrower than 50 nm.

a GaAs laser diode [Fig. 2(a)]. The vertical height resolution in these experiments was better than 1 nm. The optical resolution of our aluminium-coated tips was tested by recording a reflection mode image of a standard AFM test grating with a line spacing of 463 nm [Fig. 2(b)]. Here, laser light is transmitted through a NSOM fibre probe with an aperture of <50 nm, reflected off the grating surface, collected with a microscope objective and detected in the far field with a photomultiplier. The reflected light intensity is shown as a function of the tip position. A linescan along the line indicated in the two-dimensional picture shows structures that are narrower than 50 nm. We note that the image contrast relies at least in part on topographic changes of the surface structure.

The structure of the QWR sample studied here is shown schematically in Fig. 3. The sample was grown by MBE on patterned GaAs(311) substrates along the sidewall of 15–20 nm high mesa stripes oriented along [01-1]. In these structures the formation of a sidewall QWR was found to arise from the preferential migration of Ga atoms from both the mesa top and the mesa bottom towards the sidewall.¹³ The GaAs substrate was patterned by using optical lithography and wet chemical etching and covered with a 50 nm thick GaAs buffer

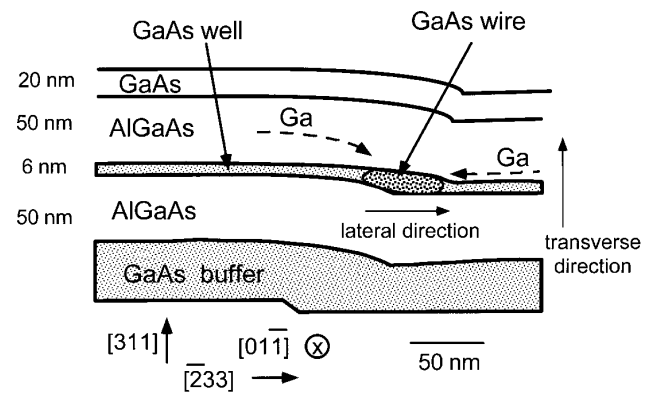


Figure 3. Schematic of the sidewall quantum wire structure. The sample is grown on a patterned GaAs(311) substrate with 15 nm high mesa stripes oriented along the [01-1] direction. Formation of GaAs quantum wires with a lateral dimension of 50 nm and a vertical dimension of 12 nm is due to the preferential migration of Ga atoms, as indicated by the dashed arrows, during the growth of the 6 nm GaAs quantum well. The GaAs quantum well is sandwiched between two 50 nm AlGaAs layers. The structure is capped with a 20 nm GaAs layer.

layer, a 50 nm $\text{Al}_{0.5}\text{Ga}_{0.5}\text{As}$ lower barrier layer and a nominally 6 nm thick GaAs QW layer. At the sidewall of the mesa, the Ga atom migration process develops a smooth convex-curved surface profile enclosing thicker wire-like regions of GaAs. This GaAs layer is covered with a 50 nm $\text{Al}_{0.5}\text{Ga}_{0.5}\text{As}$ upper barrier and a 20 nm GaAs cap layer. The structure was characterized by AFM, transmission electron microscopy (TEM) and cathodoluminescence spectroscopy.^{7,13}

RESULTS AND DISCUSSION

Micro-photoluminescence spectroscopy and electronic structure

Prior to performing near-field PL experiments, the sample was characterized by micro-photoluminescence (μ -PL) spectroscopy in Ref. 7. In these experiments a spatial resolution of ~ 1.5 μm was obtained by using a confocal imaging system and the sample was excited with 1 mW output from an Ar^+ laser emitting at 2.41 eV. For excitation of the flat part of the mesa structure (Fig. 4(a), upper panel, dashed line) a μ -PL spectrum recorded at 8 K (dashed line) shows only one peak at 1.602 eV originating from the 6 nm thick QW. At room temperature (300 K, Fig. 4(a), upper panel, solid line), the reduced bandgap of the QW results in a red shift of the emission spectrum. The room-temperature spectrum of the QW exhibits two peaks, at 1.522 and 1.555 eV, arising from the heavy and light hole-to-conduction band transitions of the QW.

The low-temperature μ -PL spectrum for sidewall excitation (Fig. 4(a), lower panel, dashed line) shows two well-separated peaks, at 1.540 and 1.605 eV. The peak at 1.540 eV was assigned to QWR emission and that at 1.605 eV to emission from the adjacent QW. The large energy difference between the QW and QWR emission lines of ~ 62 meV indicates a pronounced confinement of quasi-one-dimensional states that should be sufficient

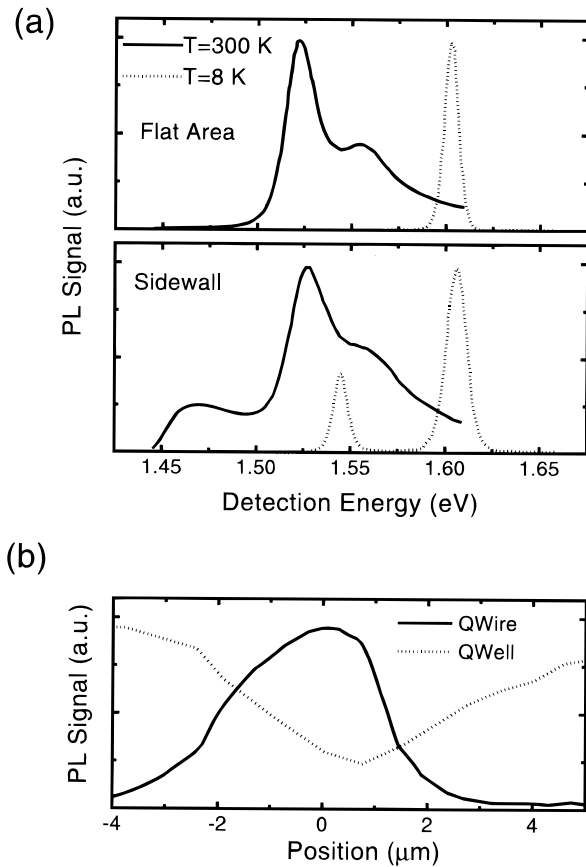


Figure 4. (a) Micro-photoluminescence (PL) spectra taken at room temperature (solid lines) and 8 K (dashed lines) from the flat part of the mesa (upper part) and at the sidewall (lower part). The additional peaks in the sidewall spectra at 1.46 eV (300 K) and 1.54 eV (8 K) are assigned to the quantum wire structure. The spatial resolution in these experiments was $\sim 3 \mu\text{m}$. (b) Micro-photoluminescence linescan at room temperature for detection at the quantum well (1.522 eV, dashed line) and at the quantum wire (1.46 eV, solid line) emission peak positions (from Ref. 7).

to keep photogenerated carriers within the wire structure even at room temperature. This is confirmed by the observation of a strong QWR emission peak, spectrally well separated from the QW emission, over the whole temperature range from 8 K up to 300 K (room temperature). In the sidewall spectrum for 300 K [Fig. 4(a), lower panel, solid line] three peaks are resolved. The quantum wire emission at 1.46 eV is well separated from the heavy-hole and light-hole QW peaks at 1.526 and 1.555 eV, respectively. We note that the heavy-hole QW emission has its maximum intensity at 1.526 eV, slightly blue-shifted relative to the corresponding peak for flat area excitation.

A room-temperature μ -PL linescan across the sample [Fig. 4(b), solid line] shows a spatial peak of QWR luminescence that is centred at the sidewall with a width of $\sim 3 \mu\text{m}$. The width of this peak is mainly limited by the spatial resolution of the confocal imaging system. Detection of the QW emission (dashed line) shows that the rise in QWR emission coincides with a decrease of the QW emission intensity. This finding suggests that the QWR emission arises from carriers photogenerated within the QW, which then get trapped and recombine within the QWR structure.

The results of the μ -PL measurements are compared to model calculations of the one-dimensional sub-band

structure of the QWR. The calculations are based on the adiabatic approximation solution⁶ of the two-dimensional Schrödinger equation. In this perturbation approach, the one-dimensional confinement results from the variation of QW thickness on a length scale much longer than the QW thickness itself, allowing a separation of the different spatial coordinates. Such a situation exists in our structures: cross-sectional TEM images⁷ indicate that the thickness of the GaAs QW varies between $\sim 5.5 \text{ nm}$ and 13 nm along the lateral y -direction [Fig. 5(a), open circles]. This variation of QW thickness extends over a range of $> 100 \text{ nm}$, which is much larger than the maximum QW thickness. The room-temperature lateral confinement energies $\varepsilon_i(y)$ ($i = \text{carrier type}$) at the lowest QW level were calculated in the effective-mass approximation using a finite-well model with $\Delta E_v/\Delta E_g = 0.67$. In Fig. 5(a), the confinement energies of electrons (solid circles), heavy holes (solid squares) and light holes (solid triangles) are plotted *vs.* the lateral coordinate y . The resulting lateral potentials $U_i(y)$ were approximated by

$$U_i(y) = \varepsilon_i(0) + [\varepsilon_i(\infty) - \varepsilon_i(0)] \tanh^2(y/2w) \quad (1)$$

where w is a measure of the effective width of the lateral well thickness variation. To reproduce the results plotted in Fig. 5(a), a value of $w = 28 \text{ nm}$ was chosen. The energy levels $E_{i,n}$ of the quantum wire sub-bands n , measured from the band edge of the bulk material, are then given as¹⁴

$$E_{i,n} = \varepsilon_i(\infty) - (\hbar^2/2m_i w^2) \times \langle -(2n-1) + 1 + \{2m_i w^2 [\varepsilon(\infty) - \varepsilon(0)]/\hbar^2\}^{1/2} \rangle^2, \quad n = 1, 2, 3 \dots \quad (2)$$

Here, m_i denote the respective effective masses. The calculated QWR probability densities for the first three electron levels are shown in Fig. 5(b), indicating the lateral extension of the QW wavefunctions. For a QW thickness of 5.5 nm , the adiabatic approximation predicts a transition energy for the first $1e \rightarrow 1hh$ interband transition of 1.610 eV at 8 K, which, considering a two-dimensional excitonic binding energy of $\sim 12 \text{ meV}$, is in fair agreement with the μ -PL experiment. For the QWR the corresponding transition energy is 1.556 eV , again somewhat larger than the observed value of 1.540 eV . At room temperature, the calculated transition energies are 1.516 eV for the flat area QW and 1.462 eV for the QWR. The predicted energies neglecting excitonic effects are much closer to the experimentally observed values than at low temperature.

We point out that the resolution of $\sim 1.5 \mu\text{m}$ obtained with the confocal imaging used in the μ -PL experiments was not sufficient to record a PLE spectrum of the QWR sample because of the small geometric filling factor of the wires relative to the surrounding QW.

Near-field spectroscopy

Both PL and PLE spectra of the sample at room temperature were investigated by near-field spectroscopy.

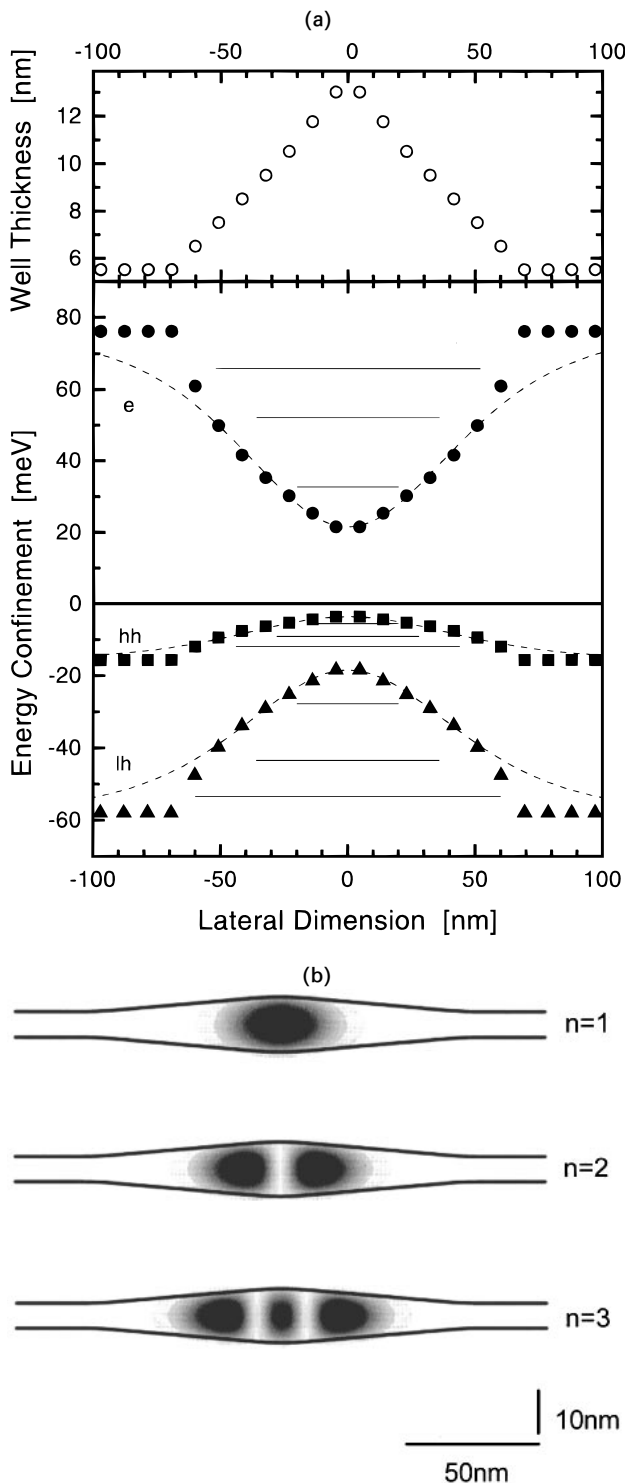


Figure 5. (a) Energetics of the quantum wire structure. Cross-sectional TEM images indicate that the thickness of the GaAs layer varies along the lateral direction between ~ 5.5 nm and 13 nm (open circles). The solid symbols denote the corresponding confinement energies for electrons (circles), heavy holes (squares) and light holes (triangles). Dashed lines are model potentials calculated from Eqn. (1). Lateral electron and heavy- and light-hole sub-band levels calculated from Eqn. (2) are shown as solid lines. (b) Probability density $|\Psi|^2$ of the electron wavefunction for the first three confined levels on a linear gray scale in relation to the shape of the quantum wire structure.

Spatially resolved measurements demonstrate that the different emission bands originate from different areas of the sample and give information on processes of carrier diffusion and trapping. In the following, we first

present the PL results, followed by a discussion of the PLE data and of the carrier exchange between QW and QWR.

Spatially resolved PL measurements. In a first set of near-field PL experiments, the sample was excited by an HeNe laser (photon energy = 1.959 eV) transmitted through a near-field probe with an aperture diameter of < 200 nm. The luminescence from the sample was collected with a microscope objective in reflection geometry. Excitation at 1.959 eV generates carriers in high-lying states in both the QW and QWR, but not in the AlGaAs barriers. The PL of the sample was detected for various detection energies between 1.40 and 1.60 eV. In Fig. 6, the detected PL intensity is plotted as a function of the tip position. The scan range in these images is $8 \mu\text{m} \times 8 \mu\text{m}$, with a pixel of $0.1 \mu\text{m}$. The images have been recorded under identical excitation conditions and the data are shown without filtering or normalization. In these images, the black and white areas correspond to zero and maximum PL intensity, respectively. The images for detection energies of 1.45 and 1.47 eV clearly show the correlation of the QWR emission with the location of the wire. The emission appears relatively homogeneous over the entire length of the QWR, confirming the high structural quality of the sample. A detailed analysis, however, reveals slight non-uniformities in the wire emission.

Images were also recorded with detection at higher energies of 1.52–1.60 eV. Results are presented in Fig. 7, which shows a plot of the PL intensity $PL(E_{\text{det}}, y)$ as a function of detection energy E_{det} and as a function of tip position along the lateral direction y , i.e. perpendicular to the wire structure centred at $y = 0$. The spectrum was recorded at 200 spatial positions, separated by 50 nm and 30 spectral positions between 1.43 and 1.59 eV. The spectral resolution was ~ 1.5 nm (FWHM). Several distinct regions are resolved in the spatially resolved PL spectrum:

- (1) The QWR emission PL_{QWR} at 1.46 eV shows a pronounced maximum around $y = 0$, i.e. at the location of the QWR. However, there is a weaker component of QWR luminescence observed for tip positions well separated from the QWR. This spatially broad QWR luminescence is resolved more clearly on a PL linescan recorded at $E_{\text{det}} = 1.46$ eV, shown in Fig. 8(a). The occurrence of this signal is related to carrier diffusion, as will be discussed below.
- (2) The PL emission from the GaAs QW centred at 1.522 eV is observed on the flat areas of the mesa top and mesa bottom. The QW emission intensity $PL_{\text{f-QW}}(y)$ remains approximately constant for y more than $3 \mu\text{m}$ on the mesa bottom and for y less than $-3 \mu\text{m}$ on the mesa top and decreases for tip positions closer to the sidewall QWR, indicating an efficient carrier capture into the wire.
- (3) In addition to contributions (1) and (2), we observed a peak in the near-field PL spectrum located at $y = 0$ and spectrally centred at 1.526 eV, i.e. at the photon energy of QW emission. This is in sharp contrast to the μ -PL linescan for detection at 1.52 eV [Fig. 4(b), dashed line], which showed a *minimum* of the PL signal at the location of the QWR structure. The near-field PL spectrum alone does not contain enough information to assign this peak but

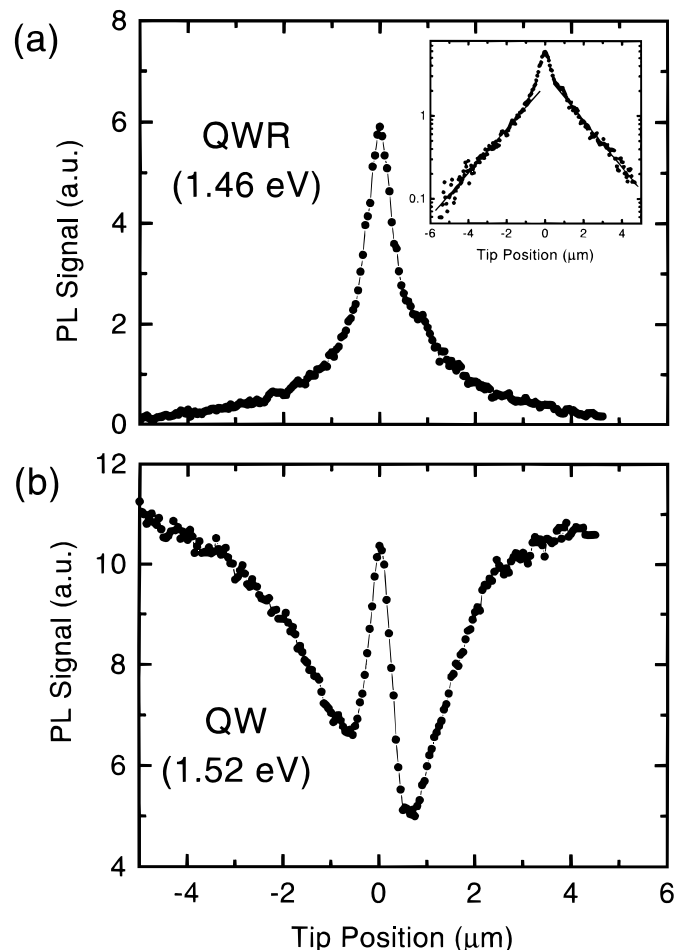


Figure 8. (a) Near-field photoluminescence (PL) linescan for detection at 1.46 eV corresponding to the detection of quantum wire (QWR) emission. The inset shows the wire emission linescan on a logarithmic scale. (b) Near-field photoluminescence linescan for detection at 1.52 eV corresponding to the detection of quantum well (QW) emission. Note the additional sidewall QW emission peak.

it will be shown below that it arises from an efficient coupling between QWR and surrounding QW states. A cross-section through the near-field PL spectrum [Fig. 8(b)] at a detection energy of 1.522 eV, corresponding to the maximum of the flat area QW emission, shows this additional QW emission at the sidewall, which could not be resolved in the μ -PL experiments, in more detail.

The PL from the QWR shows a narrow peak at the QWR centre and broad wings that extend beyond the scan range of the experiment. This intensity distribution is tentatively written as the sum of these two contributions $PL_{\text{QWR}}(y) = PL_{\text{Wing}}(y) + PL_{\text{Peak}}(y)$. The first component originates mainly from carriers generated directly in the QWR and recombining there. As will be shown below, QWR absorption should give rise to a Gaussian-shaped peak of width ~ 300 – 400 nm (FWHM). The second spatially extended signal is due to carriers generated in the QW that subsequently diffuse to the QWR and undergo recombination in its quasi-one-dimensional states. As is shown on the logarithmic plot in the inset of Fig. 8(a), the PL intensity of the wings $PL_{\text{Wing}}(y)$ decays exponentially with distance as $PL_{\text{Wing}}(y) = A_{\text{Wing}} \exp(-|y|/Ld)$. Such an exponential decay is expected for predominantly excitonic recombination.¹⁵ The decay length Ld is $1.6 \mu\text{m}$ and is assigned to the ambipolar diffusion length within the GaAs QW. From this number and a GaAs hole mobility of

$500 \text{ cm}^2 \text{ V}^{-1} \text{ s}^{-1}$,¹⁶ we estimate a carrier life-time in the QW of ~ 2 ns.

The PL from the QW exhibits two contributions, namely the flat area QW emission $PL_{\text{f-QW}}(y)$, which decreases as the excitation position approaches the QWR centre, and the narrow peak $PL_{\text{s-QW}}(y)$ at the position of the QWR. The decrease of $PL_{\text{f-QW}}(y)$ towards the QWR position should arise at least in part from the loss of carriers generated within the GaAs QW due to capture and recombination within the QWR structure. These carriers give rise to QWR luminescence and the decrease of $PL_{\text{f-QW}}$ should thus be proportional to the increase of the diffusive part of the QWR signal, PL_{Wing} , i.e. $PL_{\text{f-QW}}(y) \propto 1 - a \exp(-|y|/Ld)$, with $Ld = 1.6 \mu\text{m}$. Within reasonable accuracy, the shape of the PL line-scan [Fig. 8(b)] for QW detection and $|y| > 1 \mu\text{m}$ is reproduced by such an exponential rise if $a(y > 0)$ is taken to be $\sim 30\%$ larger than $a(y < 0)$, in order to account for the pronounced asymmetry of $PL_{\text{f-QW}}(y)$.

A comment should be made on the carrier concentration in the near-field experiments. For a rough estimate we assume that ~ 100 nW are incident on the GaAs layer and that 2% of the incident photons are absorbed. Then, $\sim 5 \times 10^9$ carriers per second are created within the GaAs layer. The mean carrier lifetime is typically of the order of 500 ps, so only a few photoexcited carriers are present simultaneously within the GaAs layer.

Photoluminescence excitation spectra. Until now, the PLE spectra of sidewall QWRs have not been determined. In the following, we present spatially and spectrally resolved PLE measurements. A near-field PLE spectrum $PLE(E_{\text{ex}}, y)$ as a function of excitation energy E_{ex} and tip position y is shown in Fig. 9. Here, the sample was again locally excited by transmitting light through the near-field probe and the far-field luminescence was dispersed in a double monochromator with a spectral resolution of 1.2 nm (FWHM). The data in Fig. 9 were recorded at a detection energy of 1.459 eV, i.e. at the maximum of the QWR emission. The tip was scanned along the lateral y -direction perpendicular to the wire structure at a rate of $2 \mu\text{m s}^{-1}$. One hundred linescans were accumulated at each of the 17 spectral excitation positions between 1.44 and 1.53 eV. No spectra were recorded between 1.455 and 1.462 eV because of the overlap with the detection window. The PLE signal is plotted at 100 spatial positions between $-5 \mu\text{m}$ and $5 \mu\text{m}$, separated by $0.1 \mu\text{m}$. The most prominent feature of the near-field PLE spectrum is the narrow structure around $y = 0$, i.e. at the location of the QWR, for excitation energies between 1.46 and 1.53 eV. Here, carriers excited in the QWR give rise to luminescence and, consequently, the intensity of the PLE spectrum at $y = 0$ is directly related to the absorption spectrum of the QWR. In Fig. 10(a) the PLE spectrum at $y = 0$ is shown. This room-temperature spectrum is quite broad, extending from 1.445 to 1.53 eV. The maximum around 1.50 eV is considerably blue-shifted compared to the QWR emission occurring at 1.459 eV [Fig. 4(a)]. A comparison with the calculations outlined above, however, indicates that the lowest QWR transition ($1e \rightarrow 1hh$) is quite close to the position of the QWR luminescence [arrow at 1.462 eV in Fig. 10(a)]. The calculations suggest that the increase of the PLE spectrum towards higher photon energies is related to absorption on several overlapping interband transitions between the heavy and light hole and the corresponding conduction sub-bands of the QWR (arrows at higher photon energies). A more detailed analysis of the spectrum will be given once results at lower temperatures have been obtained.

A linescan across the QWR structure at a fixed excitation energy of 1.48 eV and a detection energy of 1.46 eV is shown in Fig. 10(b), lower panel. This excitation energy is well below the bandgap of the 6 nm flat area QW, and carrier generation occurs only through resonant excitation of the QWR. The spatial width of the PLE signal is $\sim 260 \text{ nm}$ (FWHM) and even though the experiment has been repeated several times with NSOM fibre probes of different apertures, we were not able to record a PLE linescan with a significantly better spatial resolution. We therefore believe that the width of the QWR PLE signal is not given by the aperture size of the NSOM fibre probe but by the intrinsic properties of the QWR sample. This is supported by a simple estimate. The QWR is covered by a 50 nm AlGaAs barrier and a 20 nm GaAs cap layer with a refractive index of ~ 3.5 . This corresponds to a vacuum penetration length of $\sim 250 \text{ nm}$, which the light transmitted through the fibre probe has to traverse before reaching the QWR. The maximum attainable resolution should be of the order of this vacuum penetration length and thus $\sim 250 \text{ nm}$. This estimate is supported by beam propagation simulations.¹⁷ Several linescans for fixed excitation

energies between 1.47 and 1.51 eV were analysed and could all be fitted to a Gaussian line-shape of width 300–400 nm (FWHM).

Two additional peaks located on the mesa top and bottom are resolved in the spatially resolved near-field PLE spectrum for excitation energies between 1.51 and 1.53 eV (Fig. 9). These arise from absorption within the flat area GaAs QW. The generated carriers diffuse within the QW and eventually get trapped and recombine radiatively within the quantum wire. The spectral shape of a cross-section through the PLE spectrum at a fixed tip position is closely linked to the absorption spectrum of the flat area QW (not shown). Based on the exponential decay of the diffusive part of the near-field PL spectrum PL_{wing} , one would expect an exponential decrease of the QW PLE signal $PLE_{\text{QW}}(y) \propto \exp(-|y|/Ld)$ with a diffusion length of $1.6 \mu\text{m}$. A linescan at a fixed excitation energy of 1.52 eV and a detection energy of $E_{\text{det}} = 1.46 \text{ eV}$ [Fig. 10(b), upper panel] shows that such behavior is evidently *not* found. While the PLE signal indeed increases with decreasing distance for $|y| > 2 \mu\text{m}$, the signal does not continue to increase for shorter distances to the QWR region. In fact, a strong asymmetric *decrease* of the PLE signal is observed as the excitation source approaches the wire. While the PLE signal decreases gradually on the mesa top ($-2 \mu\text{m} < y < 0$), a much stronger and abrupt decrease is observed on the mesa bottom for distances of $< 1.2 \mu\text{m}$ away from the wire centre. Here the PLE signal decreases almost to zero at $y = 0.6 \mu\text{m}$. This signal decrease is obviously not due to a decrease of the transport properties in this narrow region around the wire because carriers generated at much longer distances from the wire can effectively reach the wire structure.

Instead, the strong signal decrease is related to a decrease of absorption in this region. The migration of Ga atoms towards the sidewall, i.e. the process underlying the formation of the QWR during MBE growth, results in a thinning of the GaAs QW in the neighborhood of the wire. A reduced QW thickness corresponds to a smaller absorption coefficient and thus less-efficient carrier generation. On top of this effect, there should be a blue shift of the absorption edge of the thinner QW, also resulting in a weaker excitation of PL. Our results suggest that the mesa top and bottom are affected differently by the Ga atom migration. While on the mesa top the thinning extends over a larger region of almost $2 \mu\text{m}$, the thinning is restricted to a much narrower region of $\sim 1 \mu\text{m}$ on the mesa bottom. On the mesa top the asymmetric thinning increases gradually with decreasing distance from the wire, while on the mesa bottom it occurs more abruptly and is more pronounced, as is evidenced by the low PLE signal at $y = 0.6 \mu\text{m}$ and by the sharp PLE signal rise between 0.6 and $1.0 \mu\text{m}$. We note that the near-field PLE signal for near-resonance QW excitation is very sensitive to small fluctuations of the QW thickness and allows such fluctuations to be resolved with high spatial resolution. This is evidenced, for example, by the narrow $< 300 \text{ nm}$ wide peak in the PLE signal shown in Fig. 10(b) at $y = 1.2 \mu\text{m}$.

Carrier exchange between QWR and QW states. So far, we have not addressed the origin of the narrow peak in the

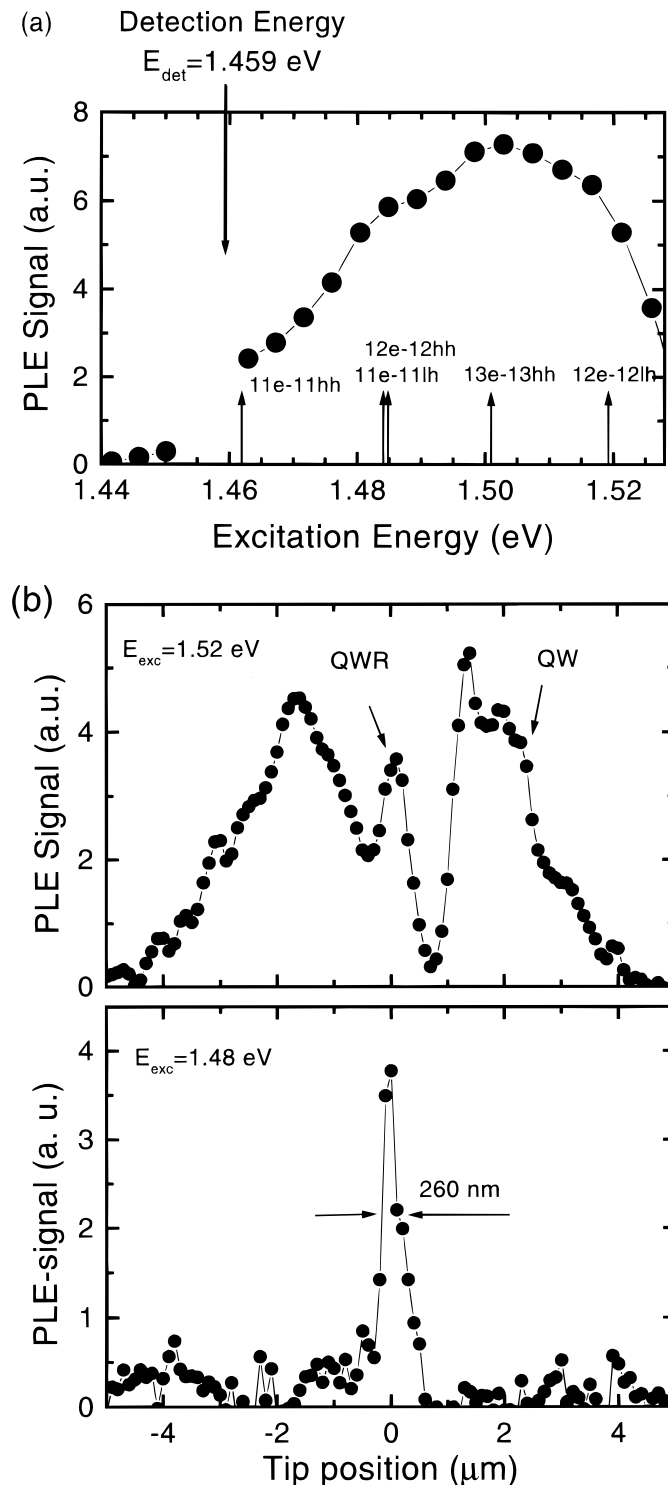


Figure 10. (a) Near-field room-temperature photoluminescence excitation (PLE) spectrum of the sidewall quantum wire (QWR) structure at a detection energy of 1.46 eV. The energetically lowest intersub-band transitions as obtained from the adiabatic approximation model calculations are indicated by black arrows. (b) Near-field room-temperature PLE linescans for excitation at 1.52 and 1.48 eV, respectively. The spatial resolution of the QWR PLE linescan of ~ 300 nm is limited by the finite thickness of the 50 nm AlGaAs barrier and the 20 nm GaAs cap layer, as described in text. QW = quantum well.

near-field PL spectrum centred at $E_{\text{det}} = 1.526$ eV [Fig. 8(b)]. We will now present two experiments that clarify this point. First, Fig. 11 shows a spatially resolved near-field PL spectrum recorded for near-resonant QWR excitation at $E_{\text{ex}} = 1.50$ eV. This excitation energy is well below the flat area QW bandgap, so that carrier generation arises only through QWR absorption. Two emission peaks are observed, the quantum wire lumi-

nescence centred at 1.46 eV and a second stronger peak centred at 1.526 eV, i.e. at higher photon energies than the excitation. The position of this high-energy PL peak coincides with the QW emission. A cross-section through the PL spectrum in Fig. 11 at $y = 0$ is similar to the QWR PL spectrum for excitation at 1.959 eV, i.e. well above the QW bandgap. This presents strong evidence that the QW peak found for excitation below the

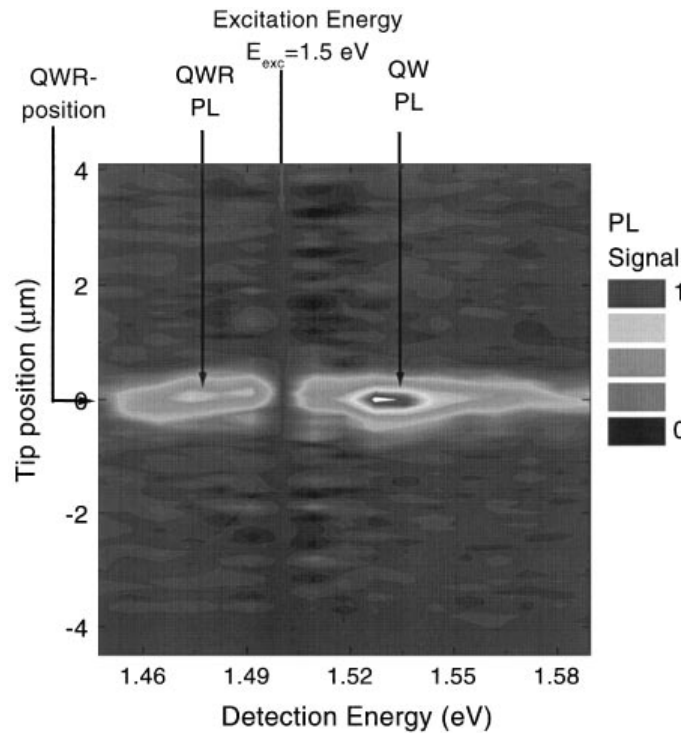


Figure 11. Near-field photoluminescence (PL) spectrum for resonant spatially resolved quantum wire (QWR) excitation at 1.5 eV. The tip was scanned along the lateral direction perpendicular to the wire structure. The PL signal (in arbitrary units) is plotted as a function of detection energy and tip position along the lateral direction perpendicular to the wire structure. The colour red corresponds to high, while purple corresponds to low PL intensity. Note the strong luminescence at the flat-area quantum well (QW) emission energy.

QW bandgap arises from a strong coupling between QWR and surrounding QW states. At room temperature, a fraction of the carriers generated within the QWR are promoted to higher energetic levels above the bandgap of the surrounding QW, where some of them recombine to give QW luminescence. Such a decapture process requires interaction with phonons or other excitations of the lattice in order to provide the energy for carrier transfer to QW states of higher energy. Very recent experiments at different sample temperatures

indicate that absorption of longitudinal optical phonons represents the main mechanism of carrier decapture. These results will be discussed in detail elsewhere.

Our interpretation of the data is further supported by resonantly exciting the QWR and spatially resolving the emission of this high-energy QW peak. This is done by using the near-field microscope in the collection mode. The QWR is excited at 1.494 eV and the resulting PL at 1.531 eV, close to the maximum of the flat-area QW emission, is collected through the near-field probe. The size of the excitation spot in this experiment is $\sim 50 \mu\text{m}$ and the spatial resolution is $\sim 300 \text{ nm}$, as defined by the sample structure. A near-field PL linescan along the y -direction, perpendicular to the wire direction (Fig. 12), shows a pronounced minimum of the PL signal near $y = 0$. This minimum in the PL signal extends over a range of $\sim 2.5 \mu\text{m}$ from about -1 to $1.5 \mu\text{m}$. The PL signal has a maximum on the flat-area mesa top and bottom $\sim 1.5 \mu\text{m}$ away from the sidewall QWR and then decreases for larger distances (not shown). The interpretation of the experiment is straightforward. Carriers are generated within the QWR and are then excited into QW states. Radiative recombination within the QW does not occur within the thinner region near the sidewall but only in the flat, QW region located at $> 1 \mu\text{m}$ away from the sidewall QWR. The increase of the bandgap energy in the thinner QW region causes a carrier drift into the lower bandgap unmodified flat QW area where recombination can occur. The decrease in PL signal for distances $|y| > 2 \mu\text{m}$ is due to the finite ambipolar diffusion length in the GaAs QW of $1.6 \mu\text{m}$. The collection mode PL signal in Fig. 12 shows an additional weak peak centred at $y = 0$. This is due to radiative QWR recombination and arises from the high-energy wing of the QWR PL spectrum.

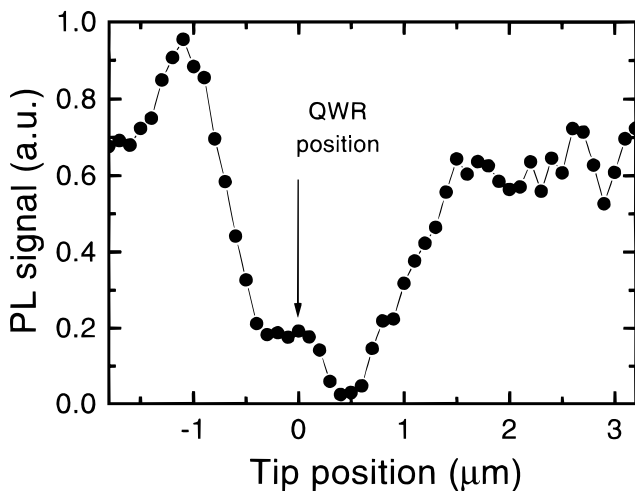


Figure 12. Collection mode near-field scanning optical microscopy (NSOM) linescan for resonant quantum wire (QWR) excitation at 1.5 eV and detection at the flat-area quantum well emission peak at 1.525 eV. The arrow denotes the position of the sidewall quantum wire as obtained from simultaneously recorded shear force images.

SUMMARY AND CONCLUSIONS

In this paper, we demonstrate the potential of near-field photoluminescence spectroscopy for characterizing the microscopic properties of semiconductor nanostructures with sub-wavelength resolution at room temperature. A combination of excitation-mode near-field PL and PLE spectroscopy and spatially resolved collection mode luminescence imaging was used in order to characterize the nanoscopic optical properties of quasi-planar QWR structures formed at the edges of patterned mesa structures on high-index GaAs surfaces. In these samples a 12 nm thick wire-like structure with a lateral width of ~50 nm is formed. The PLE and PL spectra of this wire structure were obtained with a spatial resolution of ~300 nm, which is defined by the layer structure of the particular device. Spatially resolved PL spectra separate QWR and QW and directly image the diffusion of photoexcited carriers into the QWR. Photoluminescence excitation spectra monitor the absorption spectra of the wires and the spectral positions of different interband transitions in the one-dimensional carrier system. Moreover, they provide direct information about the local thickness of the GaAs QW. In the region adjacent to the wire, the specific growth mode causes a pronounced decrease in well thickness and a corresponding increase in bandgap energy of the GaAs QW layer. Near-field

PLE spectroscopy for near-resonance excitation is shown to be particularly sensitive to such changes of the QW thickness and allows them to be resolved with sub-wavelength spatial resolution.

Evidence is found for a strong coupling between QWR and surrounding QW states. For carrier generation within the QWR a strong luminescence from the flat-area GaAs QW layer is observed, indicating the efficient population of QW states at room temperature. Such decapture processes are of fundamental importance for the successful fabrication of QWR lasers at room temperature. Here, time- and spatially resolved near-field spectroscopy shall give detailed insight into the dynamics of the coupling between one- and two-dimensional states.

Finally, we would like to state that, even though the resolution in our experiments was limited to ~300 nm, the information about the optical properties of the QWR sample that could be gained by using near-field microscopy was significantly more detailed than that obtained by using a state-of-the-art confocal imaging system. We think that near-field photoluminescence spectroscopy promises to become an invaluable tool for monitoring the nanoscopic optical properties of semiconductor heterostructures, in particular for structures located near the surface, where a resolution well below 100 nm should be possible. Such experiments are currently under way in our laboratory.

REFERENCES

1. T. Demel, D. Heitmann, P. Grambow and K. Ploog, *Appl. Phys. Lett.* **53**, 2176 (1988).
2. W. Hansen, *Adv. Solid State Phys.* **28**, 121 (1988).
3. L. N. Pfeiffer, K. W. West, H. L. Stormer, J. Eisenstein, K. W. Baldwin, D. Gershoni and J. Spector, *Appl. Phys. Lett.* **56**, 1697 (1990).
4. W. Wegscheider, L. N. Pfeiffer, M. M. Digman, A. Pinczuk, K. W. West, S. L. McCall and R. Hull, *Phys. Rev. Lett.* **71**, 4071 (1993).
5. M. Tsuchiya, H. Sugawara, T. Inoshita, A. Shimizu and H. Sakaki, *Surf. Sci.* **267**, 296 (1992).
6. E. Kapon, D. M. Hwang and R. Bhat, *Phys. Rev. Lett.* **63**, 430 (1996).
7. R. Nötzel, M. Ramsteiner, J. Menniger, A. Trampert, H.-P. Schönherr, L. Däweritz and K. H. Ploog, *Jpn. J. Appl. Phys.* **35**, L297 (1996).
8. R. Nötzel, M. Ramsteiner, J. Menniger, A. Trampert, H.-P. Schönherr, L. Däweritz and K. H. Ploog, *J. Appl. Phys.* **80**, 4108 (1996).
9. T. D. Harris, D. Gershoni, R. D. Grober, L. Pfeiffer, K. West and N. Chand, *Appl. Phys. Lett.* **68**, 988 (1996).
10. E. Betzig, P. L. Finn and J. S. Weiner, *Appl. Phys. Lett.* **60**, 2484 (1992).
11. P. C. Yang, Y. Chen and M. Vaez-Irvani, *J. Appl. Phys.* **71**, 2499 (1992).
12. Ch. Lienau, A. Richter and Th. Elsaesser, *Appl. Phys. Lett.* **69**, 325 (1996).
13. R. Nötzel, J. Menniger, M. Ramsteiner, A. Ruiz, H.-P. Schönherr and K. H. Ploog, *Appl. Phys. Lett.* **68**, 1132 (1996).
14. L. D. Landau and E. M. Lifshitz, *Quantum Mechanics*. Pergamon, Oxford (1977).
15. M. Grundmann, J. Christen, M. Joschko, O. Stier, D. Bimberg and E. Kapon, *Semicond. Sci. Technol.* **9**, 1939 (1994).
16. D. J. Wolford, W. Y. Hsu, J. D. Dow and B. G. Streetman, *J. Lumin.* **18/19**, 863 (1978).
17. A. Richter, J. W. Tomm, Ch. Lienau and J. Luft, *Appl. Phys. Lett.* **69**, 3981 (1996).